Theor Chem Account (2008) 119:57–65
DOI 10.1007/s00214-007-0270-1

REGULAR ARTICLE

Extended charge decomposition analysis and its application for the investigation of electronic relaxation

Serge I. Gorelsky · Edward I. Solomon

Received: 24 January 2007 / Accepted: 17 February 2007 / Published online: 14 March 2007

Abstract A general and comprehensive molecular orbital method for the investigation of the electronic relaxation contribution to redox processes is presented. This method is based on the population analysis of the molecular orbitals of the final electronic state in terms of the occupied and unoccupied molecular orbitals of the Koopmans' state. The DFT calculations for oxidation and reduction of transition-metal species indicate a dramatic magnitude of electronic relaxation in these systems. The passive molecular orbitals play a more significant role in electronic relaxation than the redox-active molecular orbital that directly participates in the redox process. The mechanism of electronic relaxation in the oxidation of Fe^{II} and Cu^{I} species varies from the ligand to metal 3d charge transfer (LMCT) interactions to the ligand to metal 4s,4p LMCT. For systems with significant electronic delocalization, electronic relaxation becomes smaller leading to much smaller contributions to the redox processes.

Keywords Charge decomposition analysis · Electronic relaxation · Orbital relaxation · Electronic polarization · Ionization · Oxidation · Reduction

Dedication: This contribution is to celebrate Philip Stephen's seminal contributions to theory and experiment.

S. I. Gorelsky · E. I. Solomon (✉)
Department of Chemistry, Stanford University,
Stanford, CA 94305, USA
e-mail: Edward.Solomon@Stanford.edu

S. I. Gorelsky
Centre for Catalysis Research and Innovation,
Department of Chemistry, University of Ottawa,
Ottawa, ON K1N 6N5, Canada
e-mail: sg@sg-chem.net

1 Introduction

Molecular orbital (MO) methods have always had a prominent role in the framework of computational chemistry and have permitted the development of many well-known packages to determine the electronic structure with increasing accuracy. MO methods at the density-functional theory (DFT) level have become particularly useful for molecular systems containing transition metal atoms. The wave functions thus obtained, however, require additional analysis for understanding the nature of electronic changes in chemical systems.

Recently we have developed the AOMix-CDA program [1–3] which can be used for a large number of MO analysis applications. These include Frenking's charge decomposition analysis (CDA) [4] and an extension of the method, the extended charge decomposition analysis (ECDA) [2]. The typical application of CDA and ECDA is the analysis of orbital interactions (via, for example, fragment orbital interaction diagrams) [1,5] and the evaluation of donation and back-donation in molecular complexes [1,2,5]. In AOMix-CDA, the original two-fragment, closed-shell implementation [4] of CDA has been extended to closed- and open-shell systems with multiple, closed- and open-shell fragments and ferro- and anti-ferromagnetic spin-coupling schemes.

In both CDA and ECDA, the MOs of a complex are described as the linear combinations of the occupied and unoccupied MOs of the non-interacting molecular fragments [fragment molecular orbitals (FOs)]:

$$\phi_i^{\mathrm{MO}} = \sum_{k}^{\mathrm{NF}} \sum_{a} \mathbf{c}_{ai} \phi_{a,k}^{\mathrm{FO}}, \tag{1}$$

where NF is the number of fragments.

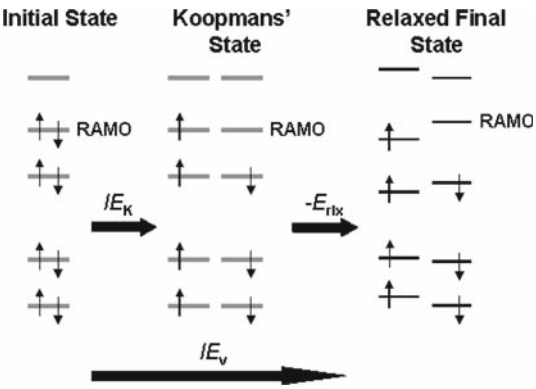

Scheme 1 Molecular-orbital description of the ionization process of the closed-shell species. In this process, an electron is removed from the redox-active molecular orbital (the RAMO) of the initial electronic state. The molecular orbitals of the initial and final electronic states are shown in *gray* and *black*, respectively. The vertical ionization energy (IE_V) is a difference between the Koopmans' ionization energy (IE_K) and the relaxation energy (E_{rlx})

In the absence of the charge transfer (CT) and electronic polarization (PL) interactions between the fragments [6,7], the occupied and unoccupied MOs (OMOs and UMOs) of the complex are described as the linear combinations of the occupied FOs (OFOs) and the linear combinations of the unoccupied FOs (UFOs), respectively:

$$\phi_i^{\mathrm{OMO}} = \sum_k^{\mathrm{NF}} \sum_a \mathbf{c}_{ai} \phi_{a,k}^{\mathrm{OFO}}, \tag{2}$$

$$\phi_i^{\mathrm{UMO}} = \sum_k^{\mathrm{NF}} \sum_a \mathbf{c}_{ai} \phi_{a,k}^{\mathrm{UFO}}. \tag{3}$$

In the presence of the CT and PL interactions, the magnitudes of the CT and PL effects are directly linked to the configuration interaction vector amplitudes of interfragment single excitations and intrafragment single excitations, respectively.

Electronic relaxation (also referred in the literature as *orbital relaxation*) is the change in electronic structure as a response to oxidation or reduction (Scheme 1). The large electronic relaxation can make significant contributions to the thermodynamics and kinetics of electron transfer [8–11]. This phenomenon can be evaluated using photoelectron spectroscopy (PES) via the intensity of CT satellite features in PES spectra [8] and using MO calculations via the analysis of the electron density redistribution after oxidation or reduction.

Recently, the detailed analysis of electronic relaxation has been performed for oxidation of $[FeCl_4]^{2-}$ and $[Fe(SR)_4]^{2-}$ using photoelectron spectroscopy and VBCI and DFT calculations [8–11]. The $[Fe(S_{Cys})_4]^{2-/1-}$ site is the simplest of iron–sulfur active sites found in electron transfer (ET) proteins, and the corresponding redox couple involves the Fe^{III} (oxidized) and Fe^{II} (reduced) high-spin states. It has been shown that valence ionization of the $[Fe^{II}L_4]^{2-}$ complexes results in dramatic charge donation from the ligands to compensate for the creation of a valence hole in the 3d shell of the Fe^{III} ion. As a result, a simple one-electron representation of the ionization process as a removal of an electron from the redox-active molecular orbital (the RAMO, Scheme 1) is insufficient and, in order to correctly describe the process, electronic relaxation (Scheme 2) that redistributes electron density back from the ligands to the metal atom must be included in the description. One of the important conclusions from this study was that a dominant contribution to electronic relaxation in the high-spin $d^6 \rightarrow d^5$ complexes comes from the *passive* β-spin MOs, i.e., orbitals that are not directly involved in the ionization process (Scheme 1). These

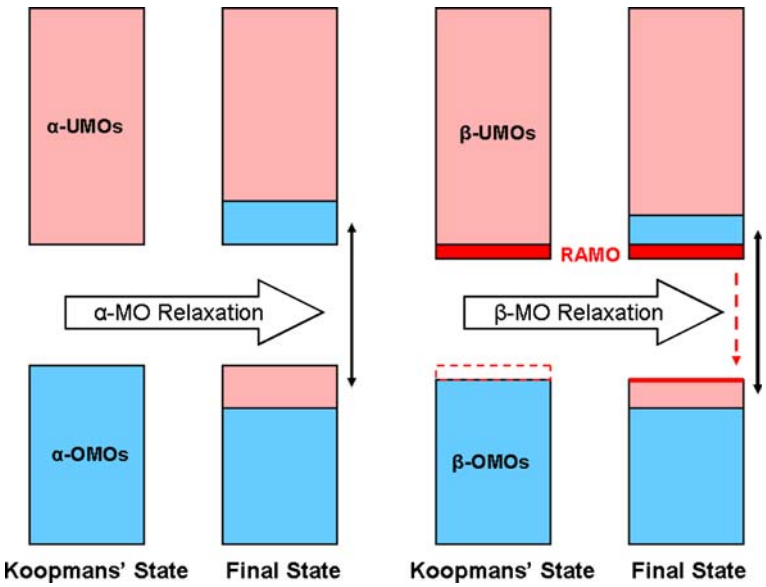

Scheme 2 Analysis of the electronic relaxation process after the ionization from the β-spin HOMO (*dashed red area*) using the contributions from the occupied MOs (OMOs, shown in *blue*), the RAMO (shown in *red*) and the other unoccupied MOs (UMO, shown in *pink*) of the Koopmans' state as the basis. The population of the unoccupied RAMO when going from the Koopmans' state to the final state is presented by a *red dashed arrow*

account for a major portion of electronic density redistribution when going from the Koopmans' state generated from the ferrous state and the ferric final state [8]. As a result, it has been proposed that the metal–ligand covalency is an important determinant of the magnitude of electronic relaxation in transition metal complexes.

In this study, we develop a general method of the MO analysis of electronic relaxation in molecular systems (both inorganic and organic) and determine the contributions of active and passive α- and β-spin orbitals (including the RAMO itself) and hole-delocalization to this process.

2 Method

In this study, the α- and β-spin MOs of the final redox state (Scheme 1) are presented as linear combinations of the α- and β-spin MOs of the initial electronic state:

$$\phi_i^{\alpha}(\text{final}) = \sum_a \mathbf{c}_{ai}^{\alpha}\phi_a^{\alpha}(\text{initial}) \tag{4}$$

$$\phi_i^{\beta}(\text{final}) = \sum_a \mathbf{c}_{ai}^{\beta}\phi_a^{\beta}(\text{initial}) \tag{5}$$

The algorithm for these transformations has been earlier described [2] but, for the analysis of electronic relaxation, the reference state is not the sum of fragment orbitals as in ordinary CDA or ECDA calculations but another electronic state of the same molecule, the Koopmans' state. This state has the same MO set as the initial electronic state except that the RAMO has a different occupancy (one electron in the initial state and zero in the Koopmans' state for oxidation and zero in the initial state and one electron in the Koopmans' state for reduction). The coefficients $\mathbf{c}_{ai}^{\alpha}$ and $\mathbf{c}_{ai}^{\beta}$ in Eqs. (4) and (5) can be converted to the changes in MO populations using the standard Mulliken scheme [12]. This allows direct evaluation of the changes in the electronic structure between the Koopmans' state and the relaxed final state in terms of contributions of individual spin-orbitals, groups of spin-orbitals (α- and β-spin MO blocks) and, if symmetry is present, MO symmetry groups via changes in their occupancies.

The MO occupancy analysis for electron relaxation can be presented graphically (Scheme 2) using the oxidation of Cu^{I} species as an example. Ionization of an electron from the RAMO (which is the β-spin HOMO for this example) creates a hole and shifts this orbital from a block of the β-spin occupied molecular orbitals (β-OMOs) to a block of the β-spin unoccupied molecular orbitals (β-UMOs). Since the OMOs of the initial electronic state (Cu^{I}) and the total electron distribution they produce are no longer optimal (in the self-consistent-field (SCF) sense) for the new redox state, the system undergoes electronic reorganization by partially populating some UMOs (including the RAMO) and de-populating some OMOs (this process is analogous to CT and PL interactions that change the electron distribution for a molecule with interacting fragments (Scheme 1 in Ref. [2]) and represented by arrows in Scheme 2); thus producing changes in the electronic distribution that lead to the relaxed final state.

Electronic relaxation energy is obtained as a difference in the electronic energies of the Koopmans' state (Scheme 1) in which the electronic density is a sum of the one-electron densities derived from the α- and β-spin MOs of the initial electronic state, Eq. (6),

$$\rho^{\text{Koopmans}} = \sum_i n_i^{\alpha}\left(\phi_i^{\alpha}(\text{initial})\right)^2 + \sum_i n_i^{\beta}\left(\phi_i^{\beta}(\text{initial})\right)^2 \tag{6}$$

(where n_i^{α} and n_i^{β} are the α- and β-spin MO occupations in the Koopmans' state), and the relaxed final electronic state (FS):

$$E_{\text{rlx}} = E_{\text{KS}} - E_{\text{FS}} \tag{7}$$

3 Computational details

Density functional theory (DFT) calculations have been performed using the *Gaussian 03* program [13]. The spin-unrestricted method was employed to model the open-shell species and, where necessary, for the closed-shell species. In all other calculations, the spin-restricted method was employed. Wave function stability calculations were performed to confirm that the calculated wave functions corresponded to the electronic ground state.

Orbital and fragment populations, spin densities and MO compositions were calculated using Mulliken population analysis (MPA) [12] using the *AOMix* program [14,15]. The analysis of the MO compositions of the final relaxed state in terms of MOs of the reference, Koopmans' state (Eqs. (4)–(5)) was performed using the *AOMix-CDA* program [1,2] which can be used with almost all widely used quantum chemistry programs (ADF [16], GAMESS, Gaussian [13], Hyperchem [17], Jaguar [18], MOPAC [19], Q-Chem [20], Spartan [21], Turbomole [22], ZINDO [23]). Mayer bond orders [24,25] were calculated using the *AOMix-L* program [1].

The species analyzed were anthracene$^{-,0,+}$($C_{14}H_{10}$), $[Ru(NH_3)_2Cl_2(bqdi)]^{-,0,+}$ where bqdi is the *o*-benzoquinonediimine ligand [5], $[Cu(tpz)(L)]^{-,0}$ where tzp is the tris (1-pyrazolyl)hydroborate ligand [1] and L is F^-, $OC_6F_5^-$ and $SC_6F_5^-$, 49-atom QM model [26] of the plastocyanin blue copper site (PCu) derived from our early PCu study [27],

the 30-atom model ($[Cu^{I}_2(SCH_3)_2(imz)_2]^{0,+}$) and 51-atom model (with the axial ligands) of the Cu_A site [28], high-spin $[Fe(SCH_3)_4]^{2-,1-}$ and $[FeCl_4]^{2-,1-}$ [8]. The structures of all species were optimized using the B3LYP exchange-correlation (XC) functional [29] with the basis sets listed in Table 1 except those of the $[Fe(SCH_3)_4]^{2-}$ and $[FeCl_4]^{2-}$ ions which were taken directly from Ref. [8]. The MOs of these latter two species were calculated using the same XC functional (BP86 [30,31]) as in the original study. Note that the extent of metal–ligand covalency is dependent on the XC functional used. The hybrid XC functionals (such as B3LYP) with the Hartree–Fock (HF) exchange added give the less covalent bonding description [32]. For the high-spin ferric compounds pure GGA functionals such as BP86 were found to give agreement with experimental data [8].

4 Results and analysis

The results of the electronic relaxation calculations are summarized in Tables 2 and 3. Table 2 contains the data related to the ionization of the species, whereas Table 3 refers to the reduction of the species. The 100% change in occupancies of the occupied and unoccupied MOs of the initial electronic state corresponds to a complete transfer of one electron from the occupied MO block to the unoccupied MO block (Scheme 2).

4.1 Ionization of high-spin ferrous species

The oxidation of the high-spin ferrous $[Fe^{II}L_4]^{2-}$ species removes an electron from the RAMO which is a metal

Table 1 Description of the computational models

Species	Symmetry	DFT model	
		XC functional	Basis set [a]
[Cu(tpz)(F)]	C_s	B3LYP	TZVP [37] for all atoms
$[Cu(tpz)(OC_6F_5)]$	C_s	B3LYP	TZVP for all atoms
$[Cu(tpz)(SC_6F_5)]$	C_s	B3LYP	TZVP for all atoms
PCu	A	B3LYP	TZVP for all atoms
$[Cu_2(SCH_3)_2(imz)_2]$	C_i	B3LYP	TZVP for Cu and S, 6-31G* other atoms
Cu_A	A	B3LYP	TZVP for Cu and S, 6-31G* other atoms
$[Ru(NH_3)_2Cl_2(bqdi)]$	C_{2v}	B3LYP	DZVP [38] for Ru and TZVP for other atoms
$[Fe(SCH_3)_4]^{2-}$	S_4	BP86	TZVP for all atoms
$[FeCl_4]^{2-}$	D_{2d}	BP86	TZVP for all atoms
Anthracene	D_{2h}	B3LYP	TZVP for all atoms

[a] All calculations were performed with pure (not Cartesian) *d* basis functions

Table 2 Electronic relaxation energies and the changes of the MO occupancies between the Koopmans' state and the relaxed final electronic state after the ionization

Species	E_{rlx} (eV)	Change of occupancies (%)[a] of		
		RAMO[b]	α-MOs	β-MOs
$[Cu^{I}(tpz)(F)]^-$	5.40	β a" 1.9	7.0 (a' 4.7, a" 2.3)	7.3 (a' 4.1, **a" 3.2**)
$[Cu^{I}(tpz)(OC_6F_5)]$	4.72	β a" 4.9	5.2 (a' 2.6, a" 2.5)	8.4 (a' 2.2, **a" 6.2**)
$[Cu^{I}(tpz)(SC_6F_5)]^-$	3.01	β a" 0.6	4.9 (a' 2.3, a" 2.6)	3.8 (a' 1.9, **a" 1.9**)
PCu^{I}	2.22[c]	β 2.3	4.5	5.4
$[Cu^{I}_2(SCH_3)_2(imz)_2]$ [d]	1.65	β a_u 0.1	3.0 (a_g 1.5, a_u 1.5)	2.4 (a_g 1.3, $\mathbf{a_u 1.1}$)
Cu_A [e]	2.03	β a 0.3	3.5	2.9
$[Ru^{II}(NH_3)_2Cl_2(bqdi)]$	2.37	β $a_2$1.2	9.8 ($a_1$1.8, $a_2$0.5, $b_1$6.9, $b_2$0.6)	5.2 ($a_1$1.5, $\mathbf{a_2 1.3}$, $b_1$1.9, $b_2$0.4)
$[Fe^{II}(SCH_3)_4]^{2-}$	5.28	β b 1.0	2.8 (a 0.4, b 1.4, e 1.0)	48.0 (a 25.4, **b 4.5**, e 18.1)
$[Fe^{II}Cl_4]^{2-}$	5.70	β a_1 11.9	1.8 (a_1 0.3, a_2 0.1, b_1 0.3, b_2 0.4, e 0.7)	23.8 ($\mathbf{a_1}$ **12.1**, a_2 0.0, b_1 0.0, b_2 1.5, e 10.1)
Anthracene	0.52	β 0.0	1.5	1.1

[a] The changes of occupancies of the MOs of different symmetry blocks are shown in parentheses. The changes in the active symmetry block (that includes the RAMO) are shown in bold
[b] These % changes correspond to the partial population of the RAMO
[c] The large PCu QM models give E_{rlx} up to 2.8 eV
[d] The 30-atom model of the Cu_A site
[e] The 51-atom model of the Cu_A site [28]

Table 3 Electronic relaxation energies and the changes of the MO occupancies between the Koopmans' state and the relaxed final electronic state after the reduction

Species	E_{rlx} (eV)	Change of occupancies[a] (%) of		
		RAMO[b]	α-MOs	β-MOs
$[Cu^{II}(tpz)(F)]$	4.78	β a" 0.1	8.2 (a' 5.3, a" 2.9)	8.2 (a' 5.3, **a" 2.9**)
$[Cu^{II}(tpz)(OC_6F_5)]$	3.43	β a" 0.6	6.4 (a' 3.2, a" 3.2)	6.4 (a' 3.2, **a" 3.2**)
$[Cu^{II}(tpz)(SC_6F_5)]$	2.82	β a" 1.1	5.6 (a' 2.6, a" 3.0)	5.6 (a' 2.6, **a" 3.0**)
$[Cu_2^{1.5}(SCH_3)_2(imz)_2]^{+}$ [c]	1.91	β a_u 0.3	3.4 (a_g1.8, a_u1.7)	3.4 (a_g1.8, $\mathbf{a_u 1.7}$)
Cu_A [d]	2.01	β a 0.3	3.7	3.7
$[Ru^{II}(NH_3)_2Cl_2(bqdi)]$	1.11	α $b_1$0.0	1.8 ($a_1$0.8, $a_2$0.2, $\mathbf{b_1 0.4}$, b_2 0.3)	3.0 (a_1 1.0, a_2 0.5, b_1 1.1, b_2 0.4)
Anthracene	0.50	α 0.1	1.1	1.3

[a] The % changes of occupancies of the MOs of different symmetry blocks are shown in parentheses. The changes in the active symmetry block (that includes the RAMO) are shown in bold

[b] These % changes correspond to the partial de-population of the RAMO

[c] The 30-atom model of the Cu_A site

[d] The 51-atom model of the Cu_A site [28]

3d-based β-spin orbital (with b_1 symmetry and the 84% Fe, 16% Cl composition for the $[Fe^{II}Cl_4]^{2-}$ ion). The resultant $[Fe^{III}L_4]^{-}$ species have an additional acceptor β-spin Fe 3d orbital for covalent bonding with the ligands and the metal-based acceptor orbitals (α- and β-spin 4s and 4p orbitals and β-spin 3d orbitals of Fe^{III}) at lower energy than the $[Fe^{II}L_4]^{-}$ species, closer to the energies of the ligand-based donor orbitals. This results in the more covalent metal–ligand bonds in the ferric species and the considerable ligand-to-metal charge transfer (LMCT) in the transition from the Koopmans' ferric state to the electronically relaxed ferric state. Although there are quantitative differences in the relaxation processes of oxidation of $[Fe^{II}Cl_4]^{2-}$ and $[Fe^{II}L_4]^{2-}$, their overall behaviors are similar. In both cases, the active symmetry block (the β-spin MO block that includes the RAMO) contributes little to electronic relaxation (Table 2), and the major role for electronic relaxation and the stabilization of the oxidized state belongs to passive β-spin MO block. The contribution of the whole α-spin MO block (2–3% change in α-spin MO occupancies, Table 2) is much less than the contribution of the β-spin MO block (24–48%). This highlights that, for the LMCT process in these species, the Fe 3d–L 3p interactions are dominant but some contributions from Fe 4s,4p –L 3p interactions exist [8].

4.2 Ionization of copper(I) species

Upon oxidation of the Cu^{I} complexes, an electron is removed from the RAMO which is a metal 3d-based β-spin orbital, as in the case of the ionization of the Fe^{II} complexes. Just like in $[Fe^{III}L_4]^{-}$, the contribution of the RAMO or the active MO block to the relaxation process is fairly small (Table 2). However, unlike the electronic relaxation in $[Fe^{III}L_4]^{-}$, the electronic relaxation in the Cu complexes involves larger contributions from the passive α-spin MO block (Table 2). This indicates that, for electronic relaxation in Cu^{II} species, the Cu^{II} 4s,4p–ligand interactions have become more significant than the Fe 4s,4p–ligand interactions in $[Fe^{III}(L)_4]^{-}$.

To study the effects of metal–ligand covalency on electronic relaxation in Cu complexes, the [Cu(tpz)(L)] series ($L = F^{-}, OC_6F_5^{-}, SC_6F_5^{-}$) was investigated (Fig. 1). Removal of an electron from the RAMO leads to more covalent Cu–L bonds and results in higher Cu–L bond orders in the Koopmans' state of these species relative to the reduced state $[Cu^{I}(tpz)(L)]^{-}$ (Table 4). For example, when going from $[Cu^{I}(tpz)(F)]^{-}$ to the Koopmans' state, the Cu–F bond order increases from 0.54 to 0.72. This increase highlights the fact that the RAMO is an anti-bonding orbital (Fig. 1) for the Cu–L donor–acceptor bond and its de-population enhances the Cu–ligand covalent bonding. The $[Cu^{II}(tpz)(F)]$ complex has the least covalent Cu^{II}–L bond, whereas the $[Cu^{II}(tpz)(SC_6F_5)]$ complex has the most covalent Cu^{II}–L bond in the series as can be seen from the atomic spin densities, β-LUMO composition and Cu–L bond orders (Table 4). The nature of the RAMO (Table 4, Fig. 1) changes from a Cu $3d_{x2-y2}$ based orbital in $[Cu^{II}(tpz)(F)]$ to a more delocalized Cu $3d_{x2-y2}$–L pπ orbital in $[Cu^{II}(tpz)(SC_6F_5)]$. As a result, in going from [Cu(tpz)(F)] to $[Cu(tpz)(OC_6F_5)]$ to $[Cu(tpz)(SC_6F_5)]$, the electronic relaxation energy decreases from 5.40 to 4.72 eV to 3.01 eV, respectively and the changes in MO populations decrease from a total (α- and β-MO blocks) of 14.3% for [Cu(tpz)(F)] to 13.6% for $[Cu(tpz)(OC_6F_5)]$ to 8.7% for $[Cu(tpz)(SC_6F_5)]$ (Table 2). As can be seen from the analysis of electron populations of the molecular fragments in the Koopmans' state and the final relaxed state (Table 4), the LMCT interactions that compensate for the hole in the RAMO in $[Cu^{II}(tpz)(L)]$ involve both the tpz and L ligands of the complex and, in most cases, the LMCT tpz $\rightarrow$ Cu^{II} interactions with the net charge donation of 0.30–0.43 e^{-} (Table 5) are more significant than the

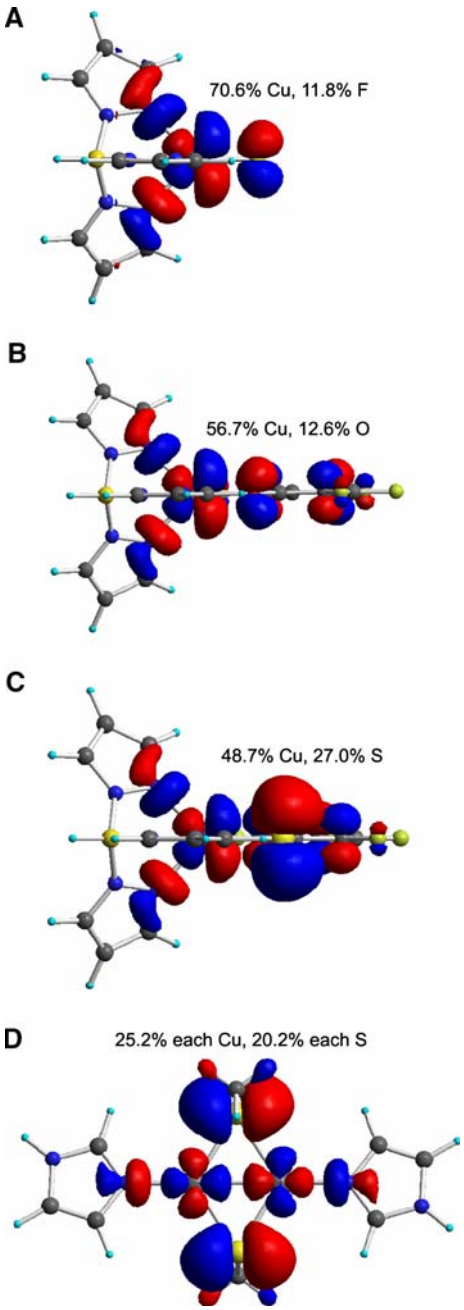

Fig. 1 β-Spin LUMO (the contour value is 0.03 a.u.) and its composition for the [Cu^{II}(tpz)(L)] complexes (**a** L = F^-, **b** L = $OC_6F_5^-$, **c** L = $SC_6F_5^-$) and (**d**) the 30-atom Cu_A model

LMCT L → Cu^{II} interactions for which the net charge donation is 0.07–0.22 e-. This ligand donation to the Cu^{II} orbitals involves population of the α- and β-spin 3d,4s,4p orbitals [with 3d orbitals receiving ~50% of the donated charge (Table 5)].

The plastocyanin blue copper site (PCu) with even more covalent Cu–thiolate bond (where the Cu and S_{Cys} contributions to the β-LUMO are from ~40% each of the two atoms) [26,27] has an even smaller E_{rlx} (Table 2). Thus, the Cu–L bond covalency plays an important role in lowering the electronic reorganization energy, and upon removal of an electron the delocalized RAMO minimizes the change of electronic structure between the Koopmans' and the relaxed final states.

This conclusion can be further evaluated by the comparison of electronic relaxation in the binuclear and mononuclear Cu sites. The binuclear Cu_A site found both in cytochrome *c* oxidase [33] and nitrous oxide reductase [34–36] functions as an ET center in these proteins and has the distorted $Cu_2(S_{Cys})_2$ diamond core with a short Cu–Cu distance (2.43 Å) [28]. In its oxidized state, Cu_A is a class III mixed-valence system ($Cu^{+1.5}Cu^{+1.5}$). The spin density is almost equally distributed between two Cu and two S_{Cys} atoms, and the β-spin LUMO very closely mirrors this description (Fig. 1) [28]. Thus, the oxidation of the reduced Cu_A cluster (with its $Cu^{+1}Cu^{+1}$ redox state) generates a mixed-valence system that requires less electronic relaxation (E_{rlx} = 1.7–2.0 eV and the total changes in the MO occupancies are only 5.4–6.4%) relative to the mononuclear Cu sites with comparable Cu–L covalency (Table 2). The 30-atom QM model of the Cu_A site without the copper axial ligands has slightly smaller electronic relaxation than a more extended 51-atom model with the axial ligands (see Ref. [28] for the description of these Cu_A models). This indicates a very weak effect of the axial ligands of Cu_A on electronic relaxation.

4.3 Reduction of copper (II) species

The reduction of the copper (II) species is the reverse process to the oxidation of the copper(I) species which we discussed previously. Since the nature of the RAMO for these two processes is the same, all the observations about electronic relaxation that have been made for the oxidation of the Cu^I species (a significant role of the passive α-spin MOs and the covalency/delocalization effects) also apply to the reduction of the Cu^{II} species (Table 3). However, the data in Tables 1 and 2 are not identical for two reasons. First, the oxidation data (Table 2) refer to the Cu species in their optimized reduced state geometries, whereas the reduction data (Table 3) refer to the Cu species in their optimized oxidized–redox state geometries. Second, since the Cu^I complexes are all closed-shell species, there is no spin polarization effect arising from non-equal number of the α- and β-spin electrons. Thus, the contributions to electronic relaxation from the α- and β-spin MO blocks are equal to each other.

4.4 Oxidation of low-spin ruthenium(II) species

As an interesting comparison to the oxidation of the high-spin Fe^{II} with a d^6 electronic configuration, is the oxidation of a low-spin $Ru^{II}(d^6)$ species. In the Ru species [$Ru^{II}(NH_3)_2Cl_2$(bqdi)] [5], the RAMO is a metal 4d(t_{2g})-based orbital

Table 4 Electronic structure of the $[Cu^{II}(tpz)(L)]$ complexes at their optimized geometries, the Koopmans' states after the ionization of $[Cu^{I}(tpz)(L)]^-$ and the corresponding final relaxed states

Species	SD	SD	BO	Composition of β-LUMO (%)	
	Cu	L	Cu-L	Cu[a]	L
$[Cu^{II}(tpz)(F)]$	0.693	0.117	0.78	70.6 (d 69.4)	11.8
Koopmans' state	0.763	0.116	0.72 (0.54[b])	76.3 (d 75.8)	11.6
Final relaxed state	0.644	0.139	0.80	66.8 (d 65.8)	13.3
$[Cu^{II}(tpz)(OC_6F_5)]$	0.560	0.282	0.90	56.7 (d 55.4)	29.5
Koopmans' state	0.703	0.203	0.70 (0.44[b])	70.3 (d 69.4)	20.3
Final relaxed state	0.504	0.383	0.85	51.1 (d 50.4)	38.5
$[Cu^{II}(tpz)(SC_6F_5)]$	0.472	0.378	1.20	48.7 (d 47.6)	39.0
Koopmans' state	0.513	0.416	1.16 (0.76[b])	51.3 (d 51.0)	41.6
Final relaxed state	0.437	0.460	1.18	44.9 (d 44.6)	45.7

Spin densities (SD), Mayer metal–ligand bond orders (BO) and the composition of the β-spin LUMO in terms of contributions from the Cu atom and the ligand L

[a]The Cu d orbital contributions to the β-spin LUMO are shown in parentheses

[b]The Cu^{I}-L bond orders in the reduced complexes, $[Cu^{I}(tpz)(L)]^-$

Table 5 α- and β-spin electron populations of the Cu atom and its 3d shell, the tpz and L ligands after ionization of the $[Cu^{I}(tpz)(L)]^-$ complexes

L	Spin	Cu [a]			tpz			L		
		KS	FS	Δ P	KS	FS	Δ P	KS	FS	Δ P
F	α	14.32 d 4.90	14.51 d 5.00	0.19 d 0.10	55.84	55.67	−0.17	4.84	4.82	−0.02
	β	13.56 d 4.14	13.87 d 4.35	0.31 d 0.21	55.71	55.45	−0.26	4.73	4.68	−0.05
OC_6F_5	α	14.33 d 4.92	14.51 d 5.00	0.18 d 0.08	55.77	55.61	−0.16	44.90	44.88	−0.02
	β	13.63 d 4.23	14.01 d 4.49	0.38 d 0.26	55.67	55.50	−0.17	44.70	44.50	−0.20
SC_6F_5	α	14.40 d 4.92	14.58 d 5.00	0.18 d 0.08	55.76	55.63	−0.13	48.83	48.79	−0.04
	β	13.89 d 4.41	14.14 d 4.53	0.25 d 0.12	55.69	55.52	−0.17	48.41	48.33	−0.08

KS Koopmans' state, *FS* final relaxed state, *ΔP* the difference in electron populations between the final state and the Koopmans' state

[a]The contributions from all Cu orbitals and Cu 3d orbitals are shown

(with ∼20% Cl 3p contributions) with a_2 symmetry (the HOMO of $[Ru^{II}(NH_3)_2Cl_2(bqdi)]$, Fig. 2a). Removal of an electron from this RAMO results in electronic relaxation of 2.37 eV. Here, the passive α-spin MOs play a much more important role (Table 2) than the passive β-spin MOs or the RAMO (which changes its population by only 1% when going from the Koopmans' state to the final relaxed state).

4.5 Reduction of low-spin ruthenium(II) species

In the reduction of the $[Ru^{II}(NH_3)_2Cl_2(bqdi)]$ complex, the RAMO is an anti-bonding, ligand-based orbital with b_1 symmetry (the LUMO of $[Ru^{II}(NH_3)_2Cl_2(bqdi)]$, Fig. 2b). Its composition is 65% π^* LUMO of the bqdi ligand and 31% HOMO of the metal fragment ($Ru^{II}(NH_3)_2Cl_2$). This composition of the LUMO reflects the back-donation from Ru^{II} to the bqdi ligand in this complex [5]. The population of this delocalized RAMO by an electron results in electronic relaxation of 2.01 eV and fairly minimal changes in MO populations (total of 4.8%) (Table 3). Since the extra electron enters the α-spin MO block, the β-spin MO block is now passive. The passive MO block is again more important than the active MO block or the RAMO.

4.6 Oxidation and reduction of anthracene

Anthracene ($C_{14}H_{10}$) is a typical polycyclic aromatic molecule that consists of three fused benzene rings. Its HOMO and LUMO are delocalized, non-degenerate π and π^* orbitals, respectively. These frontier MOs have 6–17% contributions from each of the 10 carbon atoms of anthracene while the remaining 4 carbon atoms (at the ring joints) contribute ∼1% each. As a result of this extensive delocalization, the removal of an electron from the β-spin HOMO (Table 2) or

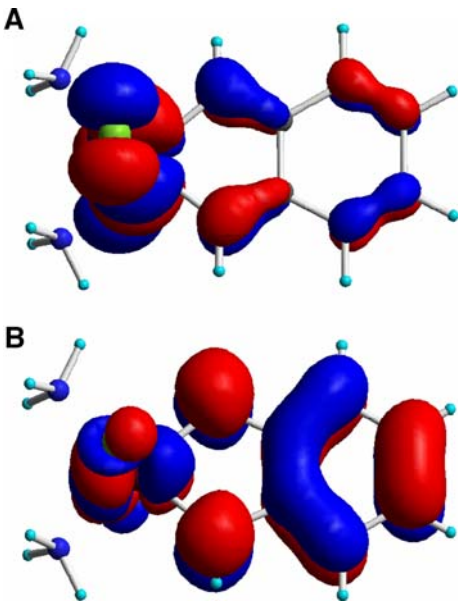

Fig. 2 The HOMO (**a**) and the LUMO (**b**) of $[Ru^{II}(NH_3)_2Cl_2(bqdi)]$ (the orbital contour value is 0.03 a.u.)

the addition of an electron to of the α-spin LUMO (Table 3) of anthracene require very little electronic relaxation of the corresponding Koopmans' states. The relaxation energies for these processes are only ~0.50 eV, and the total charges in the MO populations are only 2.4–2.6%. The changes in the RAMO occupancy during the relaxation process is 0.1% or less. This indicates that this aromatic molecular system, after oxidation or reduction, undergoes very minimal change as far as the electronic distribution is concerned. This provides an example where a simple one-electron representation of the redox process as a removal/addition of an electron from/to the RAMO is very close to valid and justifies (at least partially) the concept of the "frozen orbital" ionization in these cases.

5 Conclusions

This study prevents a molecular orbital method for the investigation of electronic structure contributions to the redox properties of different sites. We have provided theoretical data that indicate the dramatic influence of electronic relaxation on the redox properties of transition metal systems with weaker covalent bonding. The details of the mechanism for electronic relaxation depend on the electron configuration; however the common feature for all molecular systems studied is that the passive molecular orbitals play a more significant role relative to the RAMO that directly participates in the redox process. For transition metal complexes, the mechanisms of hole/electron delocalization range from the dominant ligand—metal 3d LMCT interactions and only a small contribution from ligand—metal 4s,4p LMCT interactions in the oxidation of ferrous species to a much more significant ligand—metal 4s,4p LMCT interactions in the oxidation of copper(I) species. For systems with electronic delocalization, electronic relaxation becomes less significant leading to much smaller contributions for the redox processes in conjugated delocalized systems such as anthracene.

Acknowledgments This research is supported by NSF Che-0446304 grant (E.I.S.). S.I.G. is grateful to NSERC (Ottawa) for a postdoctoral fellowship at Stanford.

References

1. Gorelsky SI, Basumallick L, Vura-Weis J, Sarangi R, Hedman B, Hodgson KO, Fujisawa K, Solomon EI (2005) Inorg Chem 44:4947
2. Gorelsky SI, Ghosh S, Solomon EI (2006) J Am Chem Soc 128:278
3. Solomon EI, Gorelsky SI, Dey A (2006) J Comput Chem 27:1415
4. Dapprich S, Frenking G (1995) J Phys Chem 99:9352
5. Rusanova J, Rusanov E, Gorelsky SI, Christendat D, Popescu R, Farah AA, Beaulac R, Reber C, Lever ABP (2006) Inorg Chem 45:6246
6. Morokuma K (1971) J Chem Phys 55:1236
7. Umeyama H, Morokuma K (1977) J Am Chem Soc 99:1316
8. Kennepohl P, Solomon EI (2003) Inorg Chem 42:679
9. Kennepohl P, Solomon EI (2003) Inorg Chem 42:689
10. Kennepohl P, Solomon EI (2003) Inorg Chem 42:696
11. Kennepohl P, Solomon EI (2004) In: McCleverty JA, Meyer TJ (eds) Comprehensive Coordination Chemistry II vol 2, pp 691. Elsevier, Amsterdam
12. Mulliken RS (1955) J Chem Phys 23:1833
13. Gaussian 03, Revision C.01, Frisch MJ, Trucks GW, Schlegel HB, Scuseria GE, Robb MA, Cheeseman JR, Montgomery Jr, JA, Vreven T, Kudin KN, Burant JC, Millam JM, Lyengar SS, Tomasi J, Barone V, Mennucci B, Cossi M, Scalmani G, Rega N, Petersson GA, Nakatsuji H, Hada M, Ehara M, Toyota K, Fukuda R, Hasegawa J, Ishida M, Nakajima T, Honda Y, Kitao O, Nakai H, Klene M, Li X, Knox JE, Hratchian HP, Cross JB, Adamo C, Jaramillo J, Gomperts R, Stratmann RE, Yazyev O, Austin AJ, Cammi R, Pomelli C, Ochterski JW, Ayala PY, Morokuma K, Voth GA, Salvador P, Dannenberg JJ, Zakrzewski VG, Dapprich S, Daniels AD, Strain MC, Farkas O, Malick DK, Rabuck AD, Raghavachari K, Foresman JB, Ortiz JV, Cui Q, Baboul AG, Clifford S, Cioslowski J, Stefanov BB, Liu G, Liashenko A, Piskorz P, Komaromi I, Martin RL, Fox DJ, Keith T, Al-Laham MA, Peng CY, Nanayakkara A, Challacombe M, Gill PMW, Johnson B, Chen W, Wong MW, Gonzalez C, Pople JA (2003) Gaussian, Inc., www.gaussian.com
14. AOMix (1997) Program for Molecular Orbital Analysis, version 6.32, Gorelsky SI, York University, Toronto, Canada. http://www.sg-chem.net
15. Gorelsky SI, Lever ABP (2001) J Organomet Chem 635:187
16. ADF, SCM (2006) Theoretical Chemistry, Vrije Universiteit, Amsterdam, The Netherlands. http://www.scm.com
17. HyperChem, Hypercube Inc., Gainesville, FL, USA. http://www.hyper.com
18. Jaguar, Schrodinger Inc., Portland, OR, USA. http://www.schrodinger.com
19. MOPAC, Stewart JJP Stewart Computational Chemistry, Colorado Springs, CO, USA. www.openmopac.net
20. Q-Chem, Q-Chem Inc., Pittsburgh, PA, USA. http://www.q-chem.com

21. Spartan, Wavefunction Inc., Irvine, CA, USA. http://www.wavefunction.com
22. Ahlrichs R, Bär M, Häser M, Horn HKC (1989) Chem Phys Lett 162:165
23. ZINDO, Zerner MC University of Florida, Gainesville, FL, USA
24. Mayer I (1986) Int J Quantum Chem 29:73
25. Mayer I (1986) Int J Quantum Chem 29:477
26. Solomon EI (2006) Inorg Chem 45:8012
27. Hansen DF, Gorelsky SI, Sarangi R, Hodgson KO, Hedman B, Christensen HEM, Solomon EI, Led JJ (2006) J Biol Inorg Chem 11:277
28. Gorelsky SI, Xie X, Chen Y, Fee JA, Solomon EI (2006) J Am Chem Soc 128:16452
29. Becke AD (1993) J Chem Phys 98:5648
30. Becke AD (1988) Phys Rev A 38:3098
31. Perdew JP (1986) Phys Rev B 33:8822
32. Szilagyi RK, Metz M, Solomon EI (2002) J Phys Chem A 106:2994
33. Iwata S, Ostermeier C, Ludig B, Michel H (1995) Nature 376:660
34. Brown K, Djinovic-Carugo K, Haltia T, Cabrito I, Saraste M, Moura JJG, Moura I, Tegoni M, Cambillau C (2000) J Biol Chem 275:41133
35. Brown K, Tegoni M, Prudencio M, Pereira AS, Besson S, Moura JJG, Moura I, Cambillau C (2000) Nature Struct Biol 7:191
36. Haltia T, Brown K, Tegoni M, Cambillau C, Saraste M, Mattila K, Djinovic-Carugo K (2003) Biochem J 369:77
37. Schafer A, Huber C, Ahlrichs R (1994) J Chem Phys 100:5829
38. Godbout N, Salahub DR, Andzelm J, Wimmer E (1992) Can J Chem 70:560